Polarimetric Backscattering Behavior of Ground Clutter at X, Ka, and W-band

A. J. Gatesman[*a], T. M. Goyette[a], J. C. Dickinson[a], R. H. Giles[a], J. Waldman[a], J. Sizemore[b], R. M. Chase[b], and W. E. Nixon[b]

[a]Submillimeter-Wave Technology Laboratory, University of Massachusetts Lowell Lowell, MA 01854

[b]U.S. Army National Ground Intelligence Center, 2055 Boulders Road Charlottesville, VA 22911

ABSTRACT

The HH and VV-polarized backscattering behavior of homogeneous ground clutter has been investigated by measuring the radar cross section per unit area of rough surface terrain. The X, Ka, and W-band behavior was investigated by analyzing ISAR imagery of 1/16th scale terrain collected in compact radar ranges operating at 160 GHz, 520 GHz, and 1.56 THz. An array of scale model ground planes was fabricated with the appropriate roughness to model relatively smooth to rough soil terrain. In addition to studying terrain backscatter as a function of surface roughness, the dependence on soil moisture content was also characterized by tailoring the dielectric constant of the scale models. The radar cross section per unit illuminated area (σ^0) was calculated as a function of elevation angle between 15° and 75°. The results of this work have been used in the fabrication of scale model ground planes for collection of radar imagery from scaled threat targets situated in realistic environments. Backscattering data are presented and compared to clutter data found in the literature.

Keywords: radar, terrain, clutter, backscattering, rough surfaces

1. INTRODUCTION

For the past 25 years, Expert Radar Signature Solutions (ERADS) under funding from the National Ground Intelligence Center (NGIC), has developed state-of-the-art scale model measurement systems to acquire radar signatures in support of a number of advanced radar applications such as automatic target recognition (ATR) systems, low-observable target evaluation, RAM development, and buried object detection. ERADS has developed fully polarimetric compact ranges at 160 GHz[1], 520 GHz[2], 1.56 THz[3] and recently, 350 THz[4] for acquisition of X, Ka, and W-band radar imagery of 1/16th, 1/35th, and 1/48th scale model targets and scenes. A new compact range operating at 2-18 GHz is also under construction for acquisition of UHF signatures of 1/35th scale target and scenes.[4]

In order to acquire realistic signatures using physical scale modeling techniques, the scaled target is usually placed on a ground plane modeling both the roughness and dielectric constant of a common

[*] correspondence: email: andrew_gatesman@uml.edu; telephone: 978-934-1365; fax: 978-452-3333

Report Documentation Page

Form Approved
OMB No. 0704-0188

1. REPORT DATE	2. REPORT TYPE	3. DATES COVERED
MAY 2005		**00-00-2005 to 00-00-2005**

4. TITLE AND SUBTITLE	5a. CONTRACT NUMBER
Polarimetric Backscattering Behavior of Ground Clutter at X, Ka, and W-band	5b. GRANT NUMBER
	5c. PROGRAM ELEMENT NUMBER
6. AUTHOR(S)	5d. PROJECT NUMBER
	5e. TASK NUMBER
	5f. WORK UNIT NUMBER
7. PERFORMING ORGANIZATION NAME(S) AND ADDRESS(ES) **University of Massachusetts Lowell,Submillimeter-Wave Technology Laboratory,175 Cabot Street,Lowell,MA,01854**	8. PERFORMING ORGANIZATION REPORT NUMBER
9. SPONSORING/MONITORING AGENCY NAME(S) AND ADDRESS(ES)	10. SPONSOR/MONITOR'S ACRONYM(S)
	11. SPONSOR/MONITOR'S REPORT NUMBER(S)

12. DISTRIBUTION/AVAILABILITY STATEMENT
Approved for public release; distribution unlimited

13. SUPPLEMENTARY NOTES
The original document contains color images.

14. ABSTRACT

15. SUBJECT TERMS

16. SECURITY CLASSIFICATION OF:			17. LIMITATION OF ABSTRACT	18. NUMBER OF PAGES	19a. NAME OF RESPONSIBLE PERSON
a. REPORT	b. ABSTRACT	c. THIS PAGE			
unclassified	**unclassified**	**unclassified**		**12**	

battlefield environment (sand, soil, asphalt, concrete, etc.). The necessary dielectric scaling technology[5,6,7] has been developed to model non-metallic components of the targets as well as ground terrain simulating various environments in which targets of interest may be deployed. Proper modeling of the target-ground interaction is necessary if signature data collected from such compact ranges are to be exploited for automatic target recognition efforts, programming of smart munitions/weapons, and testing of predictive codes.

Though ERADS signature measurement capability is typically used for acquisition of ISAR imagery of ground targets, it can be used as a powerful tool for studying radar scattering from ground terrain itself. This paper examines the X, Ka, and W-band backscattering behavior of homogeneous, rough, soil surfaces by using 1/16th scale terrain and compact ranges operating at 160 GHz, 520 GHz, and 1.56 THz. The elevation angle, θ, is defined here such that $\theta = 90°$ is normal incidence and the backscattering coefficient, σ^o, is defined as the radar cross section (m^2) per unit area (m^2) illuminated by the radar and is expressed in units of dB.

2. FABRICATION OF SCALE MODEL ROUGH SURFACES

An array of 27 ground planes was fabricated for the clutter study. Nine ground planes were required per radar band for modeling three roughness values and three soil water contents. The 15-in.-diameter rough surfaces were prepared by casting dielectrically tailored plastics into molds with the appropriate rough surface. Full-scale soil terrain can have rms roughness values, *s*, which vary from approximately 0.5 mm for very smooth soil surfaces to 40 mm for a freshly plowed field.[8] The range of rms roughness studied here extended from 2.5 mm to 11.6 mm (full-scale) and therefore modeled only moderately rough surfaces. Table I lists the ground plane designations along with the range of surface roughness values and soil moisture contents used in the study. Figure 1 shows a typical ground plane and the three types of surface terrain used. The *ks* values of the ground planes, where $k = 2\pi/\lambda$, range from 0.52 to 23.8. Values of *ks* and center wavelengths are listed in Table II.

Table I. Ground Plane Designation

Soil water content (g/cm^3)	Full scale rms roughness values *s* (mm) 2.5 mm	7.7 mm	11.6 mm
0.001	BN, BW, CF	BO, BX, CG	BP, BY, CH
0.132	BQ, BZ, CI	BR, CA, CJ	BS, CB, CK
0.294	BT, CC, CL	BU, CD, CM	BV, CE, CN

<---15 inch dia. ground plane-->

Figure 1. Images of the scale model ground planes. The images represent 1 sq. inch of each surface.

Table II. *ks* Values and Center Wavelengths.

Terrain type	Full-scale rms roughness (mm)	X-band λ = 30.0 mm	Ka-band λ = 9.16 mm	W-band λ = 3.06 mm
low roughness	2.5 mm	0.52	1.70	5.15
medium roughness	7.7 mm	1.63	5.28	15.81
high roughness	11.6 mm	2.45	7.98	23.81

In general, soil water content does not exceed 0.4 g/cm^3, so three values below 0.4 g/cm^3, designated as low, medium, and high were chosen and their corresponding reflectivities are indicated by the dots in Figure 2. Figure 2 plots the frequency dependent reflectivity of soil using an empirical formula based on a dielectric mixing model.[9] The radar reflectivity of soil is strongly dependent on frequency as well as water content. The different response as a function of water content is due predominately to the dielectric behavior of water at these frequencies. Soil reflectivities at X, Ka, and W-band at the three chosen water contents, are listed in Table III along with their corresponding complex dielectric constants.

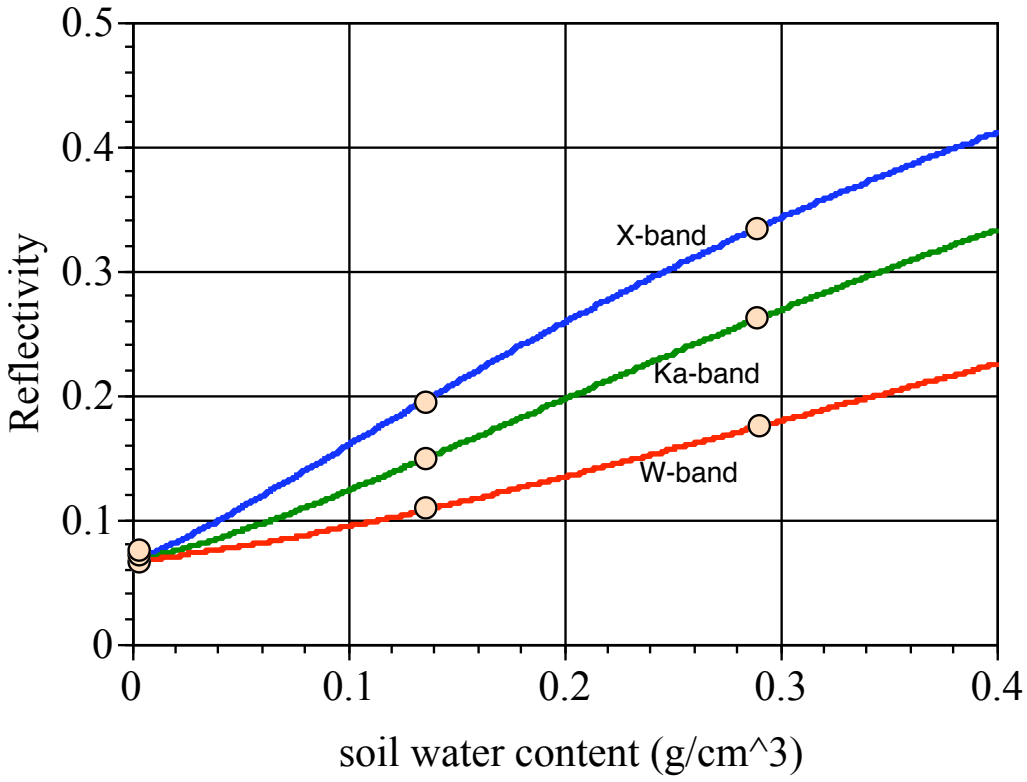

Figure 2. Normal incidence reflectivity of soil as a function of water content derived from Reference (9). The dots indicate the reflectivities of the three chosen water contents at each frequency.

Table III. Complex Dielectric Constants and Reflectivities of the Three Types of Soil at X, Ka, and W-band.

		X-band		Ka-band		W-band	
Terrain type	**soil water content (g/cm^3)**	**dielectric constant**	**Reflectivity**	**dielectric constant**	**Reflectivity**	**dielectric constant**	**Reflectivity**
low moisture	0.001	2.7 + j 0.005	6%	2.7 + j 0.007	6%	2.7 + j 0.02	7%
medium moisture	0.132	6.7 + j 1.5	20%	4.6 + j 1.8	15%	3.7 + j 1.1	11%
high moisture	0.294	13.3 + j 4.5	34%	7.1 + j 4.7	26%	4.8 + j 2.8	18%

The dielectric scaling techniques used to model the radar dielectric constant of soil at scale model frequencies was previously reported[7] and will only be summarized here. Scale modeling dielectric materials requires[10] that C_1 and C_2, which can be derived from Maxwell's equations as:

$$C_1 = \mu(\omega)\,\varepsilon(\omega)(l\,f)^2, \quad \text{and} \quad C_2 = \mu(\omega)\sigma(\omega)\,l^2\,f, \qquad \text{Eq. (1)}$$

are invariant to a change in scale factor.[11] In these equations, $\mu(\omega)$ is the material's permeability, $\varepsilon(\omega)$ is the material's bound charge dielectric constant, l is a characteristic length on the full-scale target, and f is the full-scale radar frequency. Invariance may be achieved for C_1 by decreasing the characteristic length l and increasing the frequency f by the same scale factor while maintaining the same magnetic permeability and dielectric constant. Similarly, invariance of C_2 is achieved by increasing the material's conductivity $\sigma(\omega)$ by the same scale factor. Note that the relationships for C_1 and C_2 are independent, since $\varepsilon(\omega)$ used in Eq. (1) takes only bound charges into account and not free carriers, such that $\varepsilon(\omega)$ is independent of $\sigma(\omega)$. The dielectric constant $\varepsilon(\omega)$ can still be complex and therefore describe absorption in the material. When scaling non-metallic materials ($\sigma(\omega) = 0$), invariance in C_2 is trivial, i.e. $C_2 = 0$, and the only remaining requirement (in addition to scaling l and f) is that $\varepsilon(\omega)$ and $\mu(\omega)$ of the scaled material be equal to that of the corresponding full-scale material. These requirements are summarized as:

$$\mu(\omega)_{\text{scale model}} = \mu(\omega)_{\text{full scale}}\,, \qquad \text{Eq. (2)}$$

$$\varepsilon(\omega)_{\text{scale model}} = \varepsilon(\omega)_{\text{full scale}}\,. \qquad \text{Eq. (3)}$$

Typically, full-scale and scale model materials of interest are non-magnetic ($\mu = 1$) making Eq. (2) easily satisfied. Since the complex dielectric constant of materials found on full-scale targets is typically frequency dependent, Eq. (3) requires that the scale model and full-scale material be different.

Meeting the requirement of Eq. (3) is typically accomplished by using epoxy resins and silicone-based materials loaded with specific amounts of powdered agents (silicon, carbon, aluminum, copper, stainless steel, etc.) to achieve the full-scale dielectric constant at the scale model frequency. In this work, –325 mesh carbon powder was added to a polyurethane thermoset plastic to fabricate materials with the required dielectric properties at the scaled frequencies. Figure 3 shows how the front surface THz reflectivity of polyurethane plastic can be varied as a function of carbon powder loading. These dielectric scaling techniques were used to prepare the array of scale model ground planes with the reflectivity listed in Table III.

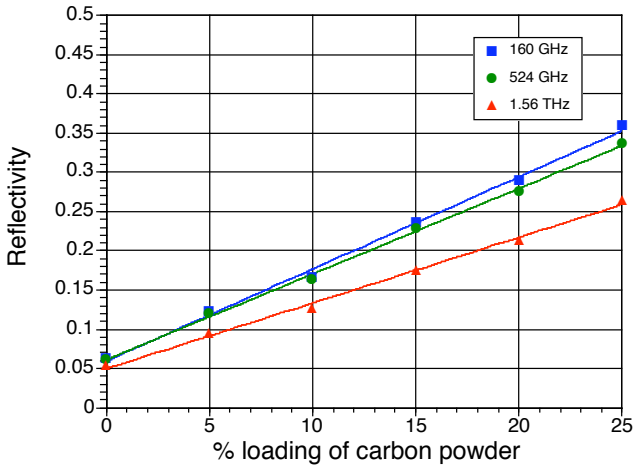

Figure 3. Reflectivity of polyurethane plastic as a function of carbon powder loading.

3. ISAR IMAGERY AND IMAGE ANALYSIS

3.1 Collection of ISAR Imagery

The ground planes were imaged using standard inverse synthetic aperture radar techniques resulting in well calibrated, high signal-to-noise, slant plane imagery. The 15-inch-diameter ground planes were mounted on low radar cross section pylons and properly oriented in azimuth and elevation in the quiet zone of the compact range. Ground plane CN mounted in the W-band compact range is shown in Figure. 4. A single measurement consisted of collecting the ground plane's backscattered magnitude and phase as it was stepped through a ≈10° azimuth sweep while held at a fixed elevation angle. The measurements were repeated for 13 different elevation angles between 15° and 75°.

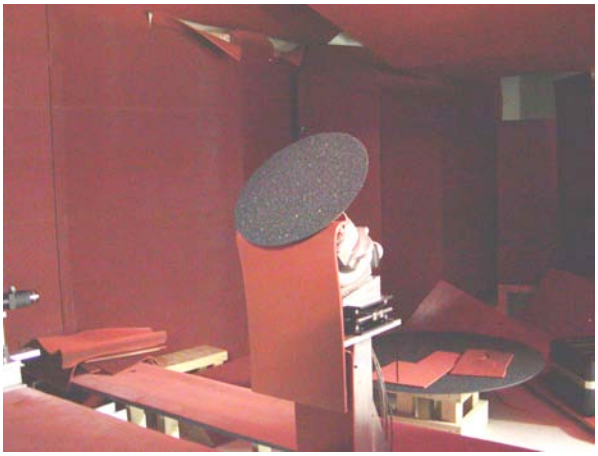
Figure 4. Ground plane CN mounted in the W-band compact range.

The resolution of the imagery depended on the bandwidth and azimuth coherent processing aperture. Frequency bandwidth dictated down-range resolution and coherent processing aperture dictated cross-range resolution. As the elevation angle was increased, the coherent processing aperture was increased so that a fixed cross-range resolution was maintained in the slant plane imagery. Center frequencies, bandwidths, and image resolutions are listed in Table IV.

Table IV. Center Frequencies, Bandwidths, and Resolutions of the Clutter Imagery.

Full-scale Frequency Band	Compact Range Center Freq.	Compact Range Bandwidth	Range Resolution (full-scale)	Cross-Range Resolution (full-scale)
X-band	160 GHz	10.5 GHz	9 inch	9 inch
Ka-band	520 GHz	15.7 GHz	6 inch	6 inch
W-band	1.56 THz	8 GHz	6 inch*	2 inch

* zero-padded to 6 inch down-range resolution

Figure 5 shows HH-polarized ISAR imagery of ground plane BR, CA, and CJ at 45° elevation. Each pixel is taken as the radar cross section for that given resolution cell. The imagery are plotted with 50 dB of dynamic range and black pixels represent 0 dBsm. The images look elliptical because they are viewed in the slant plane.

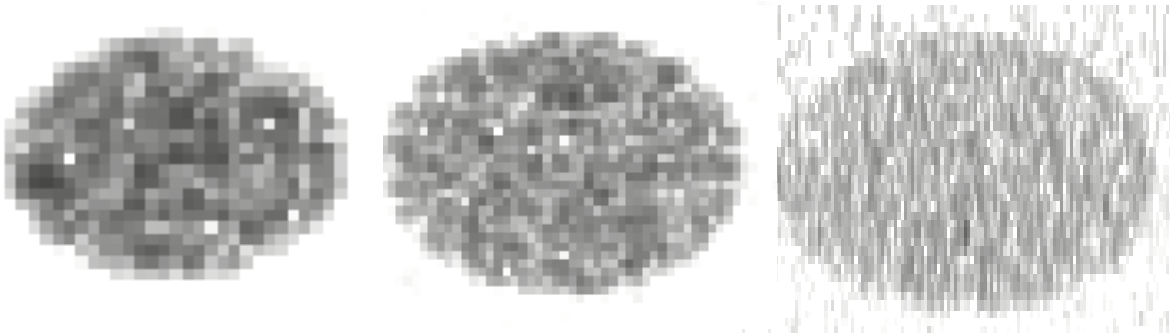

Figure 5. HH-polarized ISAR imagery of ground plane BR, CA, and CJ at 45° elevation.

3.2 General Behavior of σ^o as a Function of Elevation Angle

Calculating the backscattering coefficient σ^o consisted of incoherently summing the intensities of the pixels in an image and dividing by the area of each ground plane. The general dependence of σ^o on elevation angle can be divided into three regions:[12,13] low elevation angles, a plateau region, and high elevation angles. At low elevation, the surface will tend to appear smoother and σ^o rapidly increases with increasing angle. At large angles, σ^o also increases rapidly until it reaches a maximum at 90° (normal incidence). Between these two regions is a plateau region in which σ^0 is a weaker function of angle. HH backscatter coefficient data for all 27 ground planes are shown in Figure 6. The corresponding VV-polarized data are shown in Figure 7. The data represent averages over each roughness and each reflectivity. Overall behavior was similar to the expected general behavior of σ^o with elevation angle. However, a rapid increase in σ^o approaching normal incidence was not observed. The increase in σ^o at higher elevation angles commonly cited in the literature is possibly due to the fact that the acceptance angle of a radar's receive optics is typically several degrees wide such that some of the specularly scattered radiation is collected along with the diffuse (backscattered) radiation. A possible explanation for the lack of increase in σ^o reported here is that the data were acquired in a true far-field configuration using receivers with extremely narrow acceptance angles ($\approx 0.01°$) such that even at 75°, no specular scattering was measured.

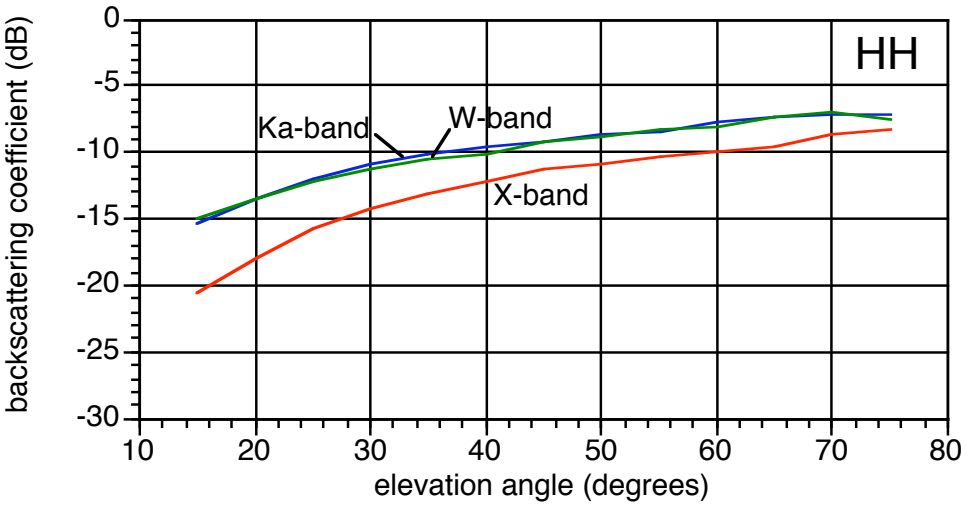

Figure 6. General behavior of σ^o_{HH} as a function of elevation angle. Data represent averages of all roughnesses and reflectivities used in the clutter study.

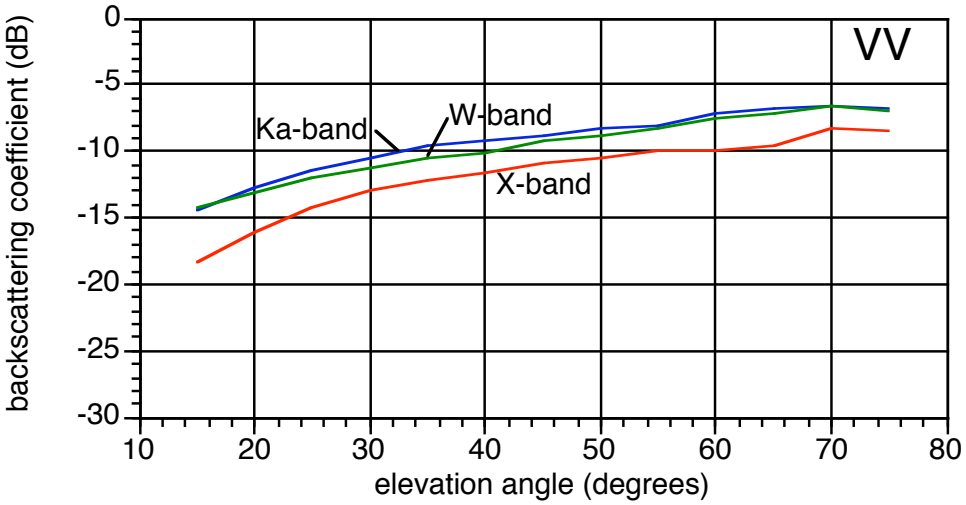

Figure 7. General behavior of σ^o_{VV} as a function of elevation angle. Data represent averages of all roughnesses and reflectivities used in the clutter study.

3.3 Dependence of Backscattering Coefficient on Polarization

The dependence of the backscattering coefficient on polarization for the highest reflectivity ground planes is shown in Figure 8. The HH and VV-polarized responses are plotted as a function of elevation angle for both the low roughness and high roughness ground planes. For the low roughness terrain, there was a significant difference between σ^o_{HH} and σ^o_{VV} at X-band, a moderate difference at Ka band, and essentially no difference at W-band. For the high roughness ground planes, however, no difference was observed in the two polarizations at any frequency. Significant differences in HH and VV-polarized radar backscatter have been observed in field measurements where greater differences are observed for smoother surfaces (e.g. asphalt, concrete) and lower elevation angles. Reference (12) shows Ka-band data where $\sigma^o_{VV}/\sigma^o_{HH}$ ratios are as high as 15 dB for concrete at an elevation angle of 20° and also indicates that $\sigma^o_{VV}/\sigma^o_{HH}$ ratios for relatively calm sea surfaces can be as high as 20 dB.

Reference (14) derives solutions for the co-polarized backscattering coefficient for horizontal and vertical polarizations assuming that; (1) the roughness is small compared to the wavelength (i.e. $ks < 1$), (2) the surface slopes of the roughness profile are relatively small, and (3) the roughness and dielectric constant are homogenous. For the given range of roughness and wavelengths chosen here, only the X-band data of the low roughness ground plane satisfy assumption (1) above. Calculating $\sigma^o_{VV}/\sigma^o_{HH}$ for this case at 20° elevation, a value of 15 dB is found. The data in Figure 8, however, only shows a ≈ 5.5 dB difference between σ^o_{HH} and σ^o_{VV} at 20° elevation, indicating poor agreement with the predictions of Reference (14). It should be noted that the ratio of $\sigma^o_{VV}/\sigma^o_{HH}$ given in Reference (14) is dependent only on the dielectric constant and elevation angle and except for the general requirement that $ks < 1$, *is not dependent on the roughness*. Reference (14) essentially predicts a $\sigma^o_{VV}/\sigma^o_{HH}$ ratio that is constant with respect to roughness and is therefore interpreted here as an upper limit on the difference between σ^o_{HH} and σ^o_{VV}. The *ks* value for the low roughness ground plane at X-band is 0.52. It is anticipated that if *ks* were to decrease, measured $\sigma^o_{VV}/\sigma^o_{HH}$ ratios would better agree with the prediction of Reference (14). The belief that $\sigma^o_{VV}/\sigma^o_{HH}$ ratios will increase as *ks* decreases is supported by the trend seen in Fig. 8 as the wavelength is increases.

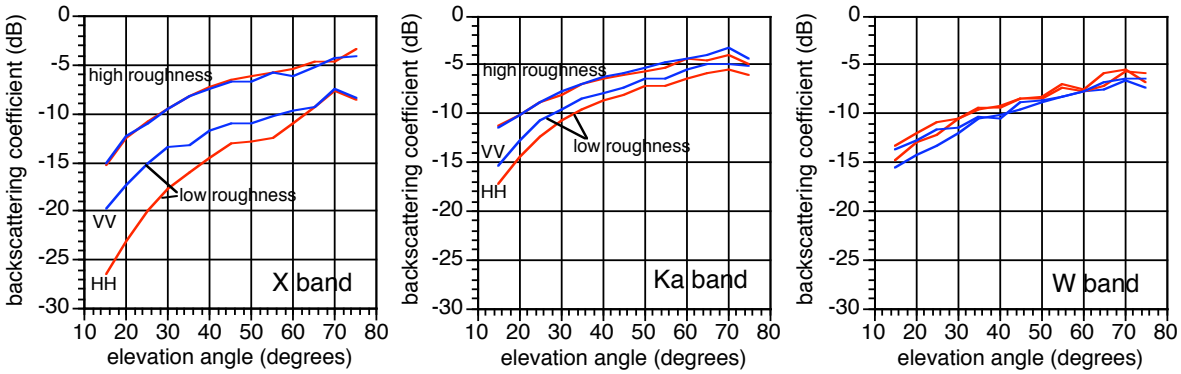

Fig. 8(a) Fig. 8 (b) Fig. 8 (c)

Figure 8. HH and VV backscattering coefficient vs. elevation angle for X-band (a), Ka-band (b), and W-band (c).

Enhanced VV-polarized backscatter is also routinely observed in our scale model target signature collections. Figure 9 shows HH and VV-polarized ISAR imagery of a 1/16th scale ground target situated on a 4-ft.-diameter ground plane modeling a dry, relatively smooth ($ks \approx 0.43$) desert-like environment at X-band. The data were acquired in a 160 GHz compact range at an elevation angle of 15°. The radar shadow cast by the target onto the ground is observable in the imagery. The imagery are displayed with 70 dB of dynamic range with black pixels representing 0 dBsm. The clutter backscatter from the VV imagery is noticeably greater than the HH image. The backscattering coefficient for the HH and VV images are -33 dB and -29 dB, respectively. It is also interesting to note that the target's HH signature is larger than its VV counterpart due to the difference in ground plane reflectivity for H and V polarization at 15° elevation.

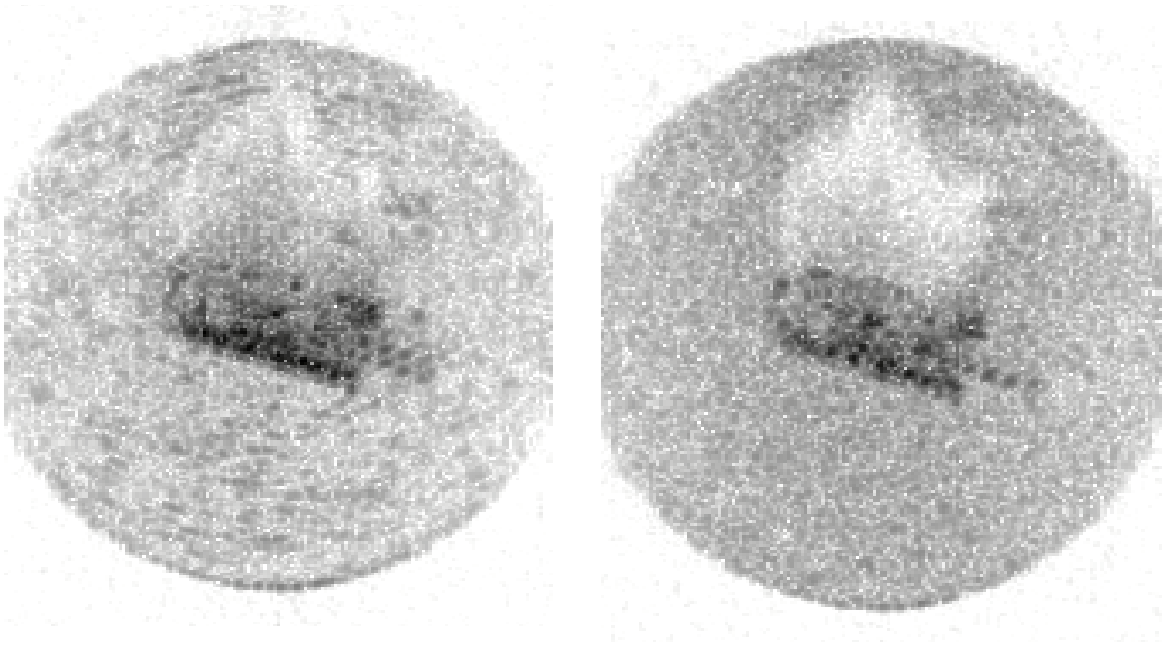

Fig. 9(a) Fig. 9(b)

Figure 9. HH (left) and VV (right) ISAR imagery of a ground target on a relatively smooth ground plane modeling desert terrain.

3.4 Dependence of Backscattering Coefficient on Soil Water Content

In the microwave and millimeter-wave region of the spectrum, the dielectric constant of completely dry soil is low and relatively constant in frequency. Water, therefore, is responsible for both soil's high dielectric constant and frequency dependence. The front surface reflectivity of soil as a function of water content was plotted in Figure 3. In addition to the rapid increase in radar reflectivity as water content increases, a strong frequency dependence is observed. For example, at the higher water contents, the reflectivity of soil at X-band is approximately 3 dB higher than at W-band.

In this study, the dependence of the backscattering coefficient on soil water content was investigated. Three water content levels denoted as low, medium, and high were used. Figure 10 shows the measured dependence of σ^o on soil water content for the medium roughness ground planes and horizontal polarization. From Figure 3, the reflectivity at X-band is expected to exhibit a stronger dependence on soil water content than at W-band. This behavior is observed in the measured data where X-band and Ka-band backscatter data show a greater change in σ^o as the soil water content is increased.

By looking at the low soil water content curves for X and W band, and noting that the ground plane reflectivities are nearly identical ($R \approx$ 6%-7%) a good estimation can be made of how σ^o varies as a function of roughness only. This roughness-only estimate says that σ^o increase by $\approx$ 3 dB from X to W-band. Competing with this effect, however, is the reduction in soil reflectivity as the frequency is increased. Figure 2 indicates a $\approx$ 3 dB drop in reflectivity between X and W-bands for soils with higher water contents. So in general, somewhat of a cancellation is expected between the two effects and therefore only a minor change in σ^o between X and W-band is expected. This behavior is indeed observed in Figure 10 where the X and W-band σ^o data are very similar as a function of elevation angle.

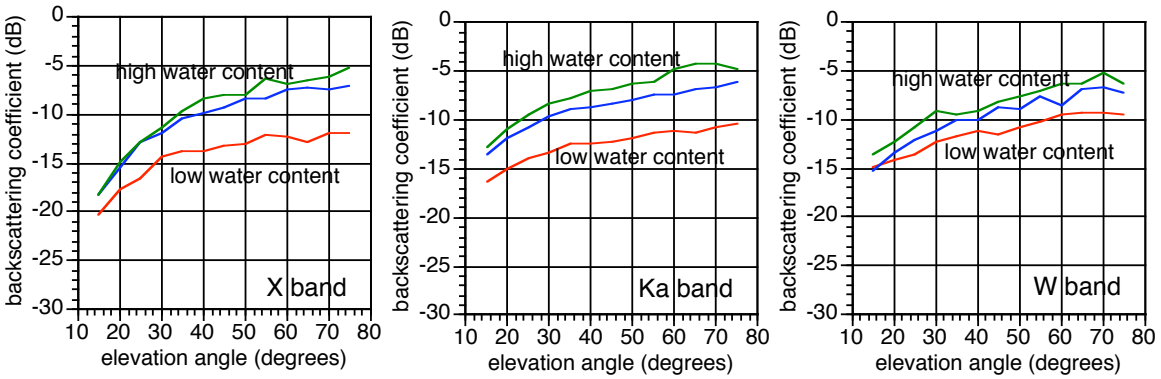

Figure 10. Dependence of backscattering coefficient on soil water content.

3.5 Agreement of Scale Model Backscatter Data with Literature Values

Agreement of the scale model X and Ka-band backscatter measurements with clutter data found in the literature was generally quite good at both relatively low and high elevation angles. Table V shows a comparison of X and Ka-band measurements with full-scale[15] measurements. The full-scale data represent averages of several different terrain types including bare soils, grasses, shrubs, road surfaces, and short vegetation. The measured values listed are taken from Figures 6 and 7, which averaged the backscattering responses over all three roughnesses and soil water contents. Measured values differed from full-scale values by no more than 1 dB. The agreement between the W-band backscatter measurements and literature data was also quite good. Table VI shows a comparison of the W-band measurements with full-scale data from Reference 8 and 16. Again, several soil types are represented with a variety of different roughnesses. Measured values differed from full-scale values by no more than 1-2 dB.

Table V. Comparison of X and Ka-band Measurements with Full-Scale Data.[15]

Frequency Band	Polarization	Elevation = 20°		Elevation = 60°	
		σ^o (literature)	σ^o (measured)	σ^o (literature)	σ^o (measured)
X-band	HH	-18 dB	-17 dB	-10 dB	-10 dB
	VV	-17 dB	-16 dB	-11 dB	-10 dB
Ka-band	HH	-15 dB	-14 dB	-6 dB	-8 dB
	VV	-14 dB	-13 dB	-7 dB	-7 dB

Table VI. Comparison of W-band Measurements with Full-Scale Data.[8,16]

Source	Terrain Type	Elevation angle	σ^o (literature)	σ^o (measured)
Ref. 8	bare soil[(a)]	15°	-15 dB (VV)	-14 dB (VV)
Ref. 8	bare soil[(b)]	20°	-14 dB (VV)	-13 dB (VV)
Ref. 16	grass and crops	32°	-11 dB [(c)]	-11 dB (VV&HH)
Ref. 8	bare soil[(b)]	45°	-7 dB (VV)	-9 dB (VV)
Ref. 16	grass and crops	73°	-7 dB [(c)]	-7 dB (VV&HH)

(a) roughness parameter ks = 8.7
(b) average over several roughnesses
(c) unknown polarization

4. CONCLUSION

The X, Ka, and W-band backscattering behavior of homogeneous ground clutter has been investigated by measuring the radar cross section per unit area of rough surface terrain. ISAR imagery were collected and backscatter data were measured as a function of elevation angle, roughness, soil moisture content, and polarization. A strong polarization dependence, in agreement with field measurements, was observed in the X-band backscatter data for the smoothest surface in the collection. All data, in general, were in excellent agreement with clutter data found in the literature indicating that millimeter-wave and microwave backscatter behavior from homogeneous terrain can be accurately modeled using physical scale modeling techniques.

ACKNOWLEDGEMENTS

This work was supported by the National Ground Intelligence Center (NGIC) under contract #DASC-01-01-C-0011.

REFERENCES

1. M. J. Coulombe, T. Horgan, J. Waldman, J. Neilson, S. Carter, and W. Nixon, "A 160 GHz Polarimetric Compact Range for Scale Model RCS Measurements," Antenna Measurements and Techniques Association (AMTA) Proceedings, Seattle, WA, October 1996.

2. M. J. Coulombe, T. Horgan, J. Waldman, G. Scatkowski, and W. Nixon, "A 520 GHz Polarimetric Compact Range for Scale Model RCS Measurements," Antenna Measurements and Techniques Association (AMTA) Proceedings, Monterey, October 1999.

3. T. M. Goyette, J. C. Dickinson, J. Waldman, W. E. Nixon, and S. Carter, "Fully Polarimetric W-band ISAR Imagery of Scale-Model Tactical Targets Using a 1.56 THz Compact Range," Proceeding of SPIE 15th Annual Inter. Symp. on Aerospace/Defense, Simulation, and Controls, Vol. 4382, Orlando, FL, April 2001.

4. T. M. Goyette, J. C. Dickinson, C. Beaudoin, A. J. Gatesman, R. H. Giles, J. Waldman, and W. E. Nixon, "Acquisition of UHF and X-Band ISAR Imagery Using 1/35th Scale Models," Proceeding of SPIE Defense and Security Symposium, Vol. 5808, Orlando, FL, March 2005.

5. R. H. Giles, A. J. Gatesman, J. Fitz-Gerald, S. Fisk, and J. Waldman, "Tailoring Artificial Dielectric Materials at Terahertz Frequencies," The Fourth International Symposium on Space Terahertz Technology, Los Angeles, CA, April 1993.

6. R. H. Giles, A. J. Gatesman, A. P. Ferdinand, and J. Waldman, "Design and Fabrication of Narrow Band Radar Absorbing Materials at Terahertz Frequencies," IEEE Proceedings from the 15th International Conference on Infrared and Millimeter Waves, Orlando, FL, Dec. 1990.

7. A. J. Gatesman, T. M. Goyette, J. C. Dickinson, J. Waldman, J. Neilson, and W. E. Nixon, "Physical Scale Modeling the Millimeter-Wave Backscattering Behavior of Ground Clutter," Proceeding of SPIE 15th Annual Inter. Symp. on Aerospace/Defense, Simulation, and Controls, Vol. 4370, Orlando, FL, April 2001.

8. F. T. Ulaby, A. Nashashibi, A. El-Rouby, E. S. Li, R. D. De Roo, K. Sarabandi, R. J. Wellman, and H. B. Wallace, "95-GHz Scattering by Terrain at Near-Grazing Incidence," IEEE Trans. on Antennas and Propagation, Vol. 46, No. 1, Jan. 1998.

9. F. T. Ulaby, R. K. Moore, and A. K. Fung, *Microwave Remote Sensing, Vol. 3*, Norwood, MA, Artech, 1982.

10. G. Sinclair, "Theory of Models of Electromagnetic Systems," Proc. Inst. Radio Eng., Vol. 36 pp. 1364-1370, 1948.

11. J. A. Stratton, *Electromagnetic Theory*, Mc-Graw-Hill Book Company, New York, 1941.

12. M. W. Long, *Radar Reflectivity of Land and Sea,* D. C. Heath and Company, 1975.

13. N. C. Currie, and C. E. Brown, *Principles and Applications of Millimeter-Wave Radar*, Artech House, Inc. Norwood, MA 1987.

14. G. T. Ruck, D. E. Barrick, W. D. Stuart, and C. K. Krichbaum, *Radar Cross Section Handbook*, *Vol. 2*, Plenum Press, New York, 1970.

15. F. T. Ulaby and M. C. Dobson, *Radar Scattering Statistics for Terrain*, Artech House, Norwood, MA, 1989.

16. N. C. Currie, R. D. Hayes, and R. N. Trebits, *Milllimeter-Wave Radar Clutter*, Artech House, Norwood, MA, 1992.